AIAA JOURNAL
Vol. 44, No. 3, March 2006

Supersonic Coaxial Jet Experiment for Computational Fluid Dynamics Code Validation

A. D. Cutler,* G. S. Diskin,† J. P. Drummond,‡ and J. A. White§
NASA Langley Research Center, Hampton, Virginia 23681

An experiment is described that has been conducted to acquire data for the validation of computational fluid dynamics codes used in the design of supersonic combustors. A coaxial nozzle has been designed to produce two uniform, pressure-matched coaxial flows at its exit. The center flow is a 95% He and 5% O_2 mixture at Mach 1.8, and the surrounding flow is air at Mach 1.8. The flow in the resultant supersonic, coaxial jet, which contains compressible mixing layers, is studied. Various methods have been employed in studying the jet flowfield, including schlieren visualization, pitot pressure, total temperature and gas sampling probe, surveys, and RELIEF velocimetry. Boundary conditions and uncertainties are characterized. VULCAN, a structured grid Navier–Stokes code, has been used to calculate the nozzle and jet flowfields, and the results are compared to the experiment.

Nomenclature

$\tilde{k}$	=	turbulent kinetic energy
M_c	=	convective Mach number
p_{amb}	=	ambient pressure
p_{exit}	=	nozzle exit pressure
p_{pit}	=	pitot pressure
$p_{ref,CJ}$	=	center-jet nozzle reference pressure
$p_{ref,coflow}$	=	coflow nozzle reference pressure
Pr_t	=	turbulent Prandtl number
Sc_t	=	turbulent Schmidt number
T_{amb}	=	ambient temperature
$T_{ref,CJ}$	=	center-jet nozzle total temperature
$T_{ref,coflow}$	=	coflow nozzle total temperature
T_t	=	total temperature
U_{nom}	=	nominal center jet velocity, 1127 m/s
u	=	x-component velocity
u'	=	fluctuation in u
x, y	=	position coordinates
$\delta_{0.0}$, $\delta_{0.99}$	=	radial distance to 1 and 99% mol fraction points respectively
σ^*	=	parameter governing diffusion of turbulent kinetic energy
χ_{He-O2}	=	mole fraction center-jet gas

Introduction

COMPUTATIONAL fluid dynamics (CFD) codes are extensively employed in the design of high-speed air-breathing engines. CFD analysis based on the Reynolds-averaged Navier–Stokes equations uses models for the turbulence that employ many ad hoc assumptions and empirically determined coefficients. Typically, these models cannot be applied with confidence to a class of flow for which they have not been validated. This paper describes one of a pair of experiments conducted at the NASA Langley Research Center that have been adopted by the NATO Research and Technology Organization (RTO) Working Group 10, Subgroup 2, as a test case for their CFD development and validation activity. This working group subgroup was formed in June 1998 to address selected technology issues related to supersonic combustion ramjets (scramjets). Much of the material reported herein, and associated CFD work, has been reported in Refs. 1–6.

Detailed experimental studies of compressible mixing have often tended to concentrate on the simplest case of a planar two-stream mixing layer, and there now exists a large body of work on this flow. Dimotakis[7] reviews much of the literature prior to 1991. Since the 1970s it was well known that the spreading (growth) rate of compressible turbulent shear layers is less than for comparable incompressible layers. Papamoschou and Roshko[8] were able to correlate the growth rate of planar two-stream mixing layers, when normalized by the growth rate of incompressible layers of the same velocity and density ratio, in terms of the "convective" Mach number. In fact, two convective Mach numbers are defined as the magnitude of the difference between the convective velocity of the mixing-layer coherent structures and one or the other of the streams, divided by the speed of sound of the respective free stream. Papamoschou and Roshko obtained the convective velocity by a simple analytical method that gave convective Mach numbers for each stream, which were nearly equal (M_c). When correlated with M_c, normalized growth rates were found to fall from 1.0 at low M_c to ~0.2 or less at $M_c > 1$. All subsequent studies, for example, Rossman et al.,[9] have confirmed this general trend. A number of measurements of convective velocity based on flow visualization have differed from the results of Papamoschou and Roshko's analytical method.[10] However, a recent study employing space–time correlation of velocity measurements finds values of convective velocity close to analytical.[11] The qualitative flow structure of compressible planar shear layers has been studied by a number of authors, for example, Clemens and Mungal,[12] who employed planar laser-induced fluorescence and planar laser Mie scattering from a condensed alcohol fog. These authors found that, as M_c is increased into the compressible range, there is a transition of the flow from nearly two-dimensional structures to more random, three-dimensional ones and a reduction of composition fluctuations. Additional detailed studies of the compressible, planar mixing layer that included velocity and fluctuating velocity measurements by laser Doppler anemometry, were conducted by Samimy and Elliott[13] and Goebel and Dutton.[14]

Baurle[15] has reviewed the state of the art in the calculation of high-speed reacting flows using CFD. The derivation of the "Favre"-averaged equations from the time-dependent Navier–Stokes, thermodynamic, and chemical kinetic equations is summarized, and the

Received 13 October 2003; revision received 8 September 2005; accepted for publication 13 September 2005.

*Professor, George Washington University, Newport News, VA 23602. Associate Fellow AIAA.
†Research Scientist, MS 468, Laser and Electro-Optics Branch. Senior Member AIAA.
‡Senior Research Scientist, MS 168, Hypersonic Airbreathing Propulsion Branch. Associate Fellow AIAA.
§Research Scientist; currently Vice President, Numerical Modeling and Simulation, Pyrodyne, Inc., Oro Valley, AZ 85737. Senior Member AIAA.

various closure equations required are identified. Various terms that must be modeled are identified, and, by reference to the literature, it is shown that improvement in the modeling of the transport of scalars, such as thermal energy and composition, is required. The current practice is often simply to model the turbulent Prandtl and Schmidt numbers Pr_t and Sc_t, which govern the ratio of the rate of turbulent momentum transport to, respectively, turbulent energy transport and turbulent mass transport, as being constant. In fact, Pr_t and Sc_t vary between 0.1 and 3 depending on the flow. Calhoon et al.,[16] in a study using large eddy simulation, showed that over the central portion of a planar two-stream mixing layer, Pr_t and Sc_t varied between 0.2 and 0.7 for $M_c = 0.27$ but were close to 0.9 at $M_c = 1.3$, depending strongly on M_c and heat release by combustion.

In a supersonic combustor, regions resembling the planar two-stream mixing layer tend to be relatively small, whereas in the greater part of an engine mixing occurs between partially mixed fuel–air plumes and "freestream" air (there being no "core" of unmixed fuel). To more closely approximate the mixing of a light-gas fuel in a supersonic combustor, while maintaining some of the simplicity of the planar mixing layer, the flow studied herein consists of a coaxial jet discharging into stagnant laboratory air, with the center jet of a light gas (a mixture of 5% O_2 and 95% He by volume) and a coflow jet of air. Both coflow and center-jet nozzles are operated pressure matched to the surrounding atmosphere. The presence of O_2 in the center-jet gas is to allow the use of an oxygen flow-tagging technique (RELIEF[17]) to obtain nonintrusive velocity measurements in the flow. Both jets are Mach 1.8, but because of the greater speed of sound of the center-jet gas, the velocity in the center jet is more than twice that of the coflow jet. The two-stream mixing layer that forms between the center jet and the coflow near the nozzle exit is compressible, with $M_c = 0.70$ (actually, the mean of the two convective Mach numbers computed by the method of Papamoschou and Roshko, as described previously). It is expected therefore that mixing rates should be reduced compared to the incompressible flow.

Two previous studies of compressible coaxial jet flows deserve mention. Gutmark et al.[18] considered the effects of convective Mach number on the mixing of circular, rectangular, and elliptical supersonic jets of various gases in a supersonic coflow of air. However, these experiments do not appear to have the required detail for code-validation purposes. Murukami and Papamoschou[19] studied a Mach-1.5 circular central jet of helium with a subsonic coflow of air. However, because of the smaller coflow jet as compared to the central jet, and rapid mixing out of the coflow, this flow is more relevant to the problem of a jet-engine exhaust flow (with bypass air) than the problem of mixing in a scramjet and does not closely resemble the flow in the present study. In addition to the experimental results, the results of sample CFD calculations of the nozzle and coaxial jet flows will be presented. The turbulent Schmidt number was varied, and results will be presented for the optimum value of 0.75.

Flow Facility

The coaxial jet-nozzle assembly is shown in Fig. 1. It is axisymmetric and consists of an outer body and a center body. The space between these bodies forms an exit nozzle (internal diameter of 60.47 mm) that forms the coflow jet, and the interior passage of the center body forms an exit nozzle (internal diameter of 10 mm) that forms the center jet. Flow entering the center body is made uniform and low turbulence by screens. The outer body consists of four parts, described from top to bottom: At the top is a conical extension ring, which is normally in place but which can be removed to provide optical or probe axis to the flow at the center-jet nozzle exit. Below that is the contoured section of the outer body, followed by a section that contains three streamlined struts that hold the center body in place. The final part is a mating flange that interfaces with the existing facility. Note that sharp corners are present at the entrance to the coflow nozzle, both at the mating flange and at the start of the center body. The large contraction ratio will likely mitigate any effect of the resulting separations on the jet flowfield.

The nozzle contours were designed using a code written for the purpose. The throat and initial expansion surface of the nozzles in the supersonic region were specified by means of a smooth function

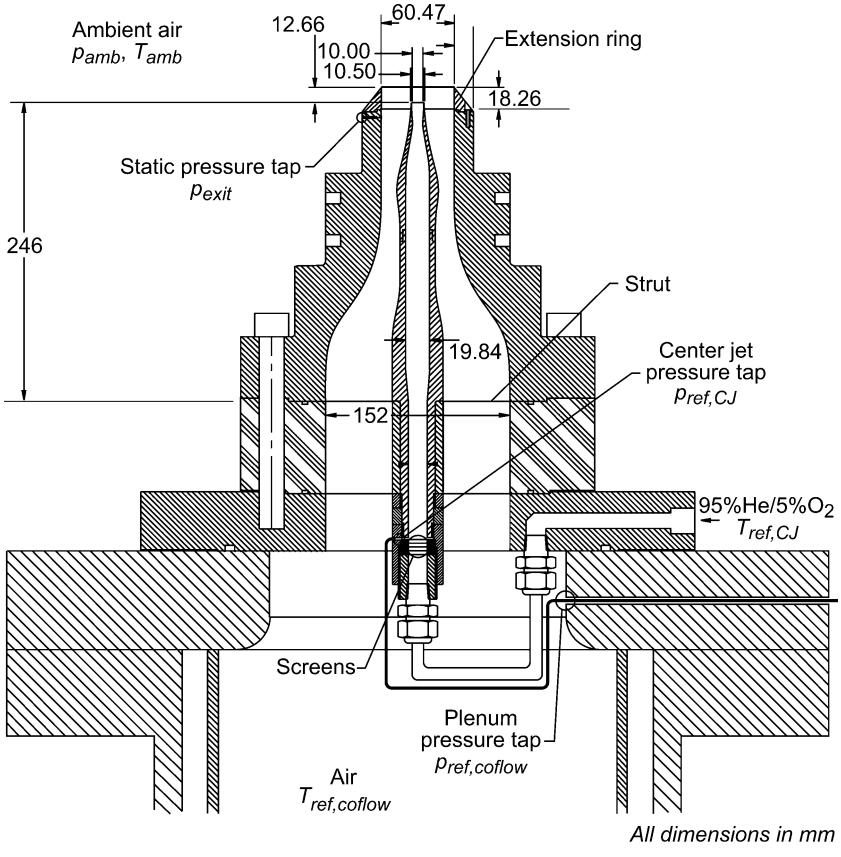

Fig. 1 Coaxial jet-nozzle assembly.

Table 1 Experimental flow parameters

Parameter	Value
$p_{\text{ref,coflow}}$ (kPa)	580 ± 4
$T_{\text{ref,coflow}}$ (K)	300 ± 6
$p_{\text{ref,CJ}}/p_{\text{ref,coflow}}$	1.060 ± 0.011
$T_{\text{ref,CJ}}/T_{\text{ref,coflow}}$	1.02 ± 0.05
$p_{\text{amb}}/p_{\text{ref,coflow}}$	0.1758 ± 0.0017
$T_{\text{amb}}/T_{\text{ref,coflow}}$	0.982 ± 0.019
$p_{\text{exit}}/p_{\text{ref,coflow}}$	0.1748 ± 0.0013

with zero second derivative at the downstream end (to ensure nearly continuous second derivatives of the nozzle surface coordinate). The flow in the supersonic region was calculated by the method of characteristics (MOC), with the remaining surface of the nozzle specified to produce one-dimensional flow at the nozzle exit. Flow conditions along the initial value line for the MOC calculation were obtained by adapting Sauer's transonic small perturbation method (see Zucrow and Hoffman[20]). The coflow nozzle is unusual in that expansion occurs on the center body while the outer surface of this nozzle is parallel to the axis. This required that Sauer's analysis be extended to account for the presence of the center body. The initial expansion surface of each nozzle was iterated to provide a nozzle-exit Mach number of 1.8.

After designing the inviscid contours of each nozzle, the nozzle boundary layers were calculated using boundary-layer codes (Harris et al.[21] and Appendix C of Wilcox[22]), assuming turbulent flow. The inviscid contours were corrected for the boundary layer by shifting them radially (toward larger flow area) by the displacement thickness. The coflow nozzle contour was truncated slightly at the downstream end, and the exit and axes of the center jet and coflow nozzle contours were aligned. The truncation was performed to provide adequate center-body wall thickness, that is, sufficient distance between the center-jet and coflow nozzle contours. It also slightly reduced the thickness of the boundary layer at the end of the coflow nozzle surface. Some small errors were made in correcting the center-jet nozzle contour for displacement thickness, and it was subsequently shown that the center-jet nozzle boundary layer was probably laminar, rather than turbulent as assumed. Consequently, as is discussed later, the Mach number of the flow at the exit of the center-jet nozzle is not quite 1.8.

The nozzle assembly is joined to the plenum of the Mixing Studies Facility, located in the laboratories of the Hypersonic Airbreathing Propulsion Branch at NASA Langley Research Center. This plenum contains porous plates for acoustic dampening and screens for flow conditioning. Air is provided to the facility from a central air station, and the He–O_2 mixture is provided to the center body from a bottle trailer containing premixed gas.

The assembly is instrumented with pressure taps: one in the center body just downstream of the screens, one in the facility plenum, and one in the outer body near the exit of the coflow nozzle (in a region where the flow has reached its exit condition). Thermocouples are located in the gas supply lines. Ambient (barometric) pressure and ambient temperature are read. The values of these various quantities during the probe surveys and their respective uncertainties (with 95% probability) are given in Table 1, and the location of these measurements and nomenclature is shown in Fig. 1. Uncertainties are due to both facility unsteadiness and variations in set point and to transducer error.

Flowfield Measurements

Various types of flowfield measurements were performed. The flow was visualized with conventional schlieren and shadowgraph. Pitot, gas-sampling, and total-temperature probes were employed to survey the flow, and the RELIEF velocity-measurement technique was used to obtain distributions of mean and fluctuating axial-component velocity.

Survey probe tips are cylindrical and cut square, with outside/inside diameters of the pitot probe of 0.64/0.36 mm respectively, and of both the gas-sampling probe and total-temperature probe of 1.27/0.76 mm. The gas-sampling probe interior passage and tubing internal diameters were sized to avoid choking the sample-gas flow, ensuring shock attachment at the probe tip. The total-temperature probe is a miniature shrouded, vented thermocouple. The probe incorporates a commercial microminiature probe consisting of a thermocouple junction at the tip of a 0.20-mm diameter "needle." Uncertainty in pitot pressure resulting from pressure transducer error is $\pm 0.5\%$. Uncertainty in total temperature resulting from thermocouple error is ± 2 K. In addition, the total-temperature probe is found to read about 1% low because of incomplete stagnation of the flow at the sensor and/or radiation losses.

The mole fraction of center-jet gas (i.e., the He-O_2 mixture) in the gas withdrawn from the flow by the gas-sampling probe, $\chi_{\text{He-O2}}$, was found in real time by a hot-film probe-based system.[23] The largest contribution to the uncertainty of the system is the manufacturer-quoted $\pm 1\%$ of full-scale uncertainty in the mass flow controller used to provide a "known" center-jet gas/air mixture to calibrate the system. Maximum uncertainty in mole fraction of center-jet gas is in the range ± 1–1.5%, but uncertainty is less than this when mole fractions are near 0.0 or 1.0. (Note that there is no uncertainty in $\chi_{\text{He-O2}}$ when the calibration mixture is known to be pure air or center-jet gas.)

The probes were mounted in a diamond-airfoil strut, and translated in the flow by a two-component stepper-motor-driven translation stage. Probe "zero" location was determined using machined fixtures mounted to the nozzle exit. Surveys were conducted across a diameter of the flow. Analysis of the data to find the best-fit center showed it to be within 0.4 mm (95% of the time) of the measured center. Thus, probe surveys are taken to pass through the axis of the jet ± 0.4 mm. The presented survey data have been shifted (by less than ± 0.4 mm) so that the best-fit center lies at $y = 0$. Resulting data are found to be almost perfectly symmetrical.

In addition to these "conventional" techniques, the RELIEF[17] (Raman excitation plus laser-induced electronic fluorescence) O_2 flow-tagging technique, illustrated in Fig. 2, has been used to provide measurements of the (instantaneous) axial component of velocity. RELIEF is a time-of-flight technique that involves two steps. The first ("tag") step involves a stimulated Raman scattering process.[24] In this process, a molecule absorbs a photon from a laser beam at one wavelength and immediately emits a second "Stokes" photon at a longer wavelength, at the same wavelength as a second, overlapping laser beam and coherent with it. Thus, the molecule is excited to an energy state that is higher than the initial state by the difference between the energy of the incident and Stokes photons. More specifically, stimulated Raman scattering is used to excite O_2 to a higher, nonequilibrium vibrational state along a line segment of the flow. Pulsed, collinear laser beams at 532 and 580 nm are generated for this purpose by passing a 200-mJ doubled Nd:YAG laser beam (10-ns pulses, 532 nm) through a 6.9-MPa Raman cell containing a 50:50 mixture of He and O_2. Stimulated Raman scattering in the Raman cell converts part of the 532-nm light to 580-nm light. The efficiency of this conversion process is improved by seeding

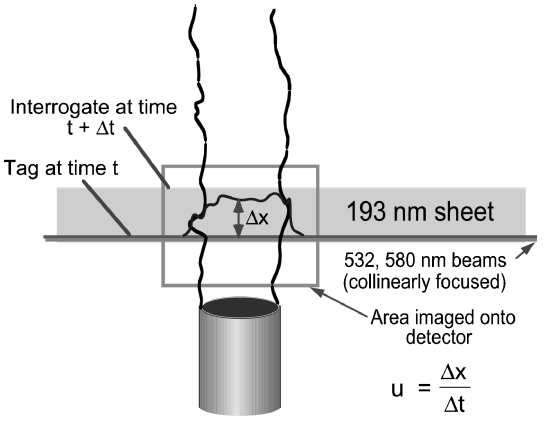

Fig. 2 RELIEF technique.

the Raman cell with a small amount of 580-nm light from a broadband dye laser pumped by the same 532-nm laser. A lens with a 50-cm focal length is used to focus the resulting collinear beams to a line in the region of the flow to be tagged. After being tagged, the line of O_2 decays from this nonequilibrium vibrational state only slowly as it convects with the flow. In the second, ("probe") step of the technique, which happens a short time after the tag step, the "tagged" O_2 is visualized by laser-induced fluorescence imaging. A pulsed, narrow-band ArF excimer laser (193 nm, 0.5 cm^{-1} line width) containing 20 mJ per pulse is tuned to a frequency that is absorbed specifically by the tagged O_2. This beam is focused to a 10-mm-high and 0.5-mm-thick sheet in the region where the tagged flow is expected to be, using cylindrical and spherical lenses. The resulting fluorescence appears immediately and is imaged using a double-intensified video-rate CCD camera, with an f/4.5 UV lens and extension rings for closeup operation. Images of the tagged flow were acquired at a rate of 5 Hz.

For each survey location, the resulting data consist of 100–128 images of displaced tagged lines, and a second set of such images acquired either at a different delay time after the tag or acquired prior to operation of the jet (i.e., with zero flow velocity). The instantaneous velocity was determined by finding the line displacement at various points along it and dividing by the probe delay time. A calibration was performed to establish the relationship between position in the image and position in space. Mean velocity $\bar{u}$ and rms fluctuation $\sqrt{u'^2}$ were obtained from the lines of instantaneous velocity. Uncertainties in this data are approximately $\pm 3\%$, due in part to uncertainty in the magnification factor between the flowfield and image and in part to uncertainty in the position of the tag line at zero time delay.

As is discussed later, the probe data exhibited a high degree of symmetry about the axis, consistent with the tight geometrical tolerances to which the model was manufactured. (Symmetry was not imposed artificially.) However, because of the relatively small amount of RELIEF data acquired and a desire to reduce the precision error in the averages, RELIEF data were reflected across the axis, effectively doubling the size of the data set. Thus, symmetry in the velocity data is imposed.

CFD Calculations

CFD calculations of the flow in the nozzle and jet field have been performed using both the Spark[25,26] and the Vulcan[27] codes. Both codes are structured, finite-volume codes that solve the Favre-averaged Navier–Stokes equations. Various turbulence models have been employed. Results of the Spark code computations are reported in Refs. 2 and 4. Selected results of the Vulcan code calculations, which are similar, are reported in Refs. 3 and 6 and also herein.

The Favre-averaged Navier–Stokes equations were solved on a structured grid using the finite-volume method. Mixtures of thermally perfect gases were assumed. Inviscid fluxes were calculated using the Kappa = one-third MUSCL (monotone upstream-centered scheme for conservation laws) scheme with the approximate Riemann solver of Roe, and viscous fluxes were evaluated using second-order central differences. A diagonalized approximate factorization scheme was used for iterating the unsteady equations in pseudotime to a steady-state solution. Coarse-to-fine grid sequencing was used on three grid levels to accelerate the development of the solution.

The grid was generated by a separate, commercial code. There are a total of 188,080 cells, distributed among five blocks. Grid points were clustered near the walls of the nozzles to resolve the boundary layers, at the exit of the center-jet nozzle to resolve the recirculation zone and shocks in the vicinity of the nozzle lip, and to a lesser degree near the axis to resolve shock reflections. The distance from the wall of the centers of the closest cells in wall units (y^+) is greater than 1.5 for all surfaces.

The walls were specified to be adiabatic and no slip. Total pressure and temperature conditions were specified at subsonic inflow/outflow planes, and the code switched to extrapolation where the outflow is supersonic. The flow is assumed to be axisymmetric. At the exterior boundary the composition is air with density of 1.177 kg/m^3 and pressure 101.3 kPa. At the coflow-nozzle inflow boundary the composition is air with total density 6.735 kg/m^3 and total pressure 580.0 kPa. At the center-jet-nozzle inflow boundary the composition is 0.7039 by mass He and 0.2961 by mass O_2, with total density 1.334 kg/m^3 and total pressure 628.3 kPa (computed from the inflow static pressure, $p_{\mathrm{ref,CJ}}$, and the area ratio between the reference plane and sonic throat, assuming quasi-one-dimensional flow). The Courant–Friedrichs–Lewy number was ramped from 0.1 to 3.0 over a few thousand iterations at each grid level. Convergence on the fine grid was relatively slow, with about 30,000 iterations required to reduce the L_2 norm of the residual by 3.5 orders of magnitude. Most calculations were carried out to 40,000 or more iterations.

The turbulence is modeled by Wilcox's 1998 high-Reynolds-number $\tilde{k}$–$\tilde{\omega}$ turbulence model,[22] including Wilcox's generalization of Pope's modification to the $\tilde{k}$–$\tilde{\varepsilon}$ model, which attempts to resolve the round jet/plane jet anomaly. The compressibility correction proposed by Wilcox is also used. The turbulent heat and mass flux are computed from the local temperature and species mass fraction gradients, and the eddy viscosity, by assuming a constant value of turbulent Prandtl number Pr_T and turbulent Schmidt number Sc_T equal to 0.75.

Results

Calculated contours of the Mach number within the nozzle and in the vicinity of the nozzle exit are shown in Fig. 3. The Mach number varies smoothly within the two nozzles. In the freestream at the exit of the center-jet nozzle, at $x = 0$, the Mach number is 1.80 ± 0.005, and at the same location in the freestream of the coflow nozzle it is 1.80 ± 0.003. As the centerbody is approached from the freestream side, at the exit, the Mach number falls slightly because of the truncation of the calculated coflow-nozzle contour. Boundary layers of significant thickness can be observed, particularly on the center body. The effects of this layer are seen in the measurements and calculations of the flow in the jet.

A typical schlieren image (with vertical knife edge) showing the jet with coflow-nozzle conical extension ring removed is Fig. 4. Vertical dark and bright bands visible in the image are due to transverse gradients of refractive index. Notice the shock-expansion waves emanating outward from the 0.25-mm-thick center-body lip. Similar waves that propagate in the center jet are not visible in the schlieren because of the low refractive index there but may be seen in the CFD calculation (Figs. 3 and 5). The continuation of these initially inward-propagating waves, after they have crossed at the axis and passed out of the center jet into the coflow air, is visible. The CFD calculation of the jet flow, Fig. 5, shows that the inward-propagating wave from the center-jet nozzle forms a normal shock where it intersects the axis. This wave intersection results in a small deficit in total

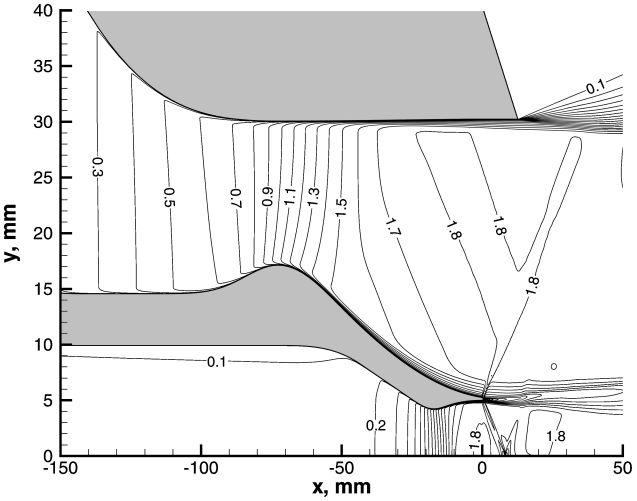

Fig. 3 Calculated contours of Mach number in the nozzle (also shows boundaries of grid blocks).

Fig. 4 Schlieren image with vertical knife edge (conical extension ring removed).

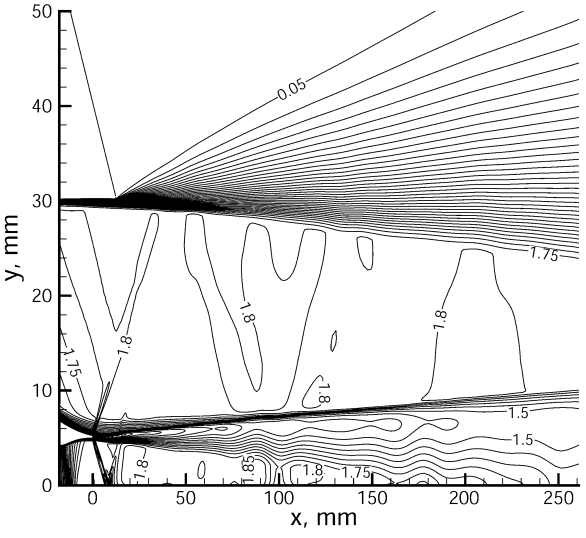

Fig. 5 Calculated contours of Mach number in the coaxial jet.

pressure at the axis that is visible downstream of the shock in both CFD and pitot pressure measurements (Figs. 6 and 7). This deficit persists as far downstream as $x = 101$ mm before being obscured by the mixing of the coflow into the center jet. Shock-expansion waves may also be seen emanating inward from the outside exit corner of the coflow nozzle. These arise because, with the extension ring removed, entrained ambient air at the nozzle exit impinges on the coflow air at 90 deg. In all other testing and also the calculation the

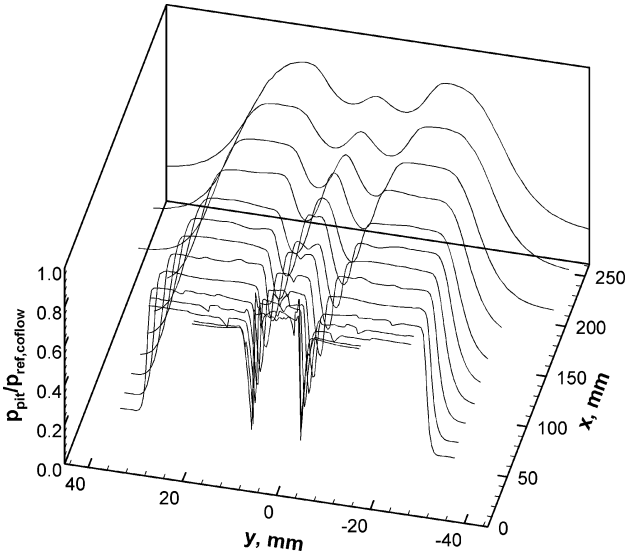

Fig. 6 Pitot pressure measurements.

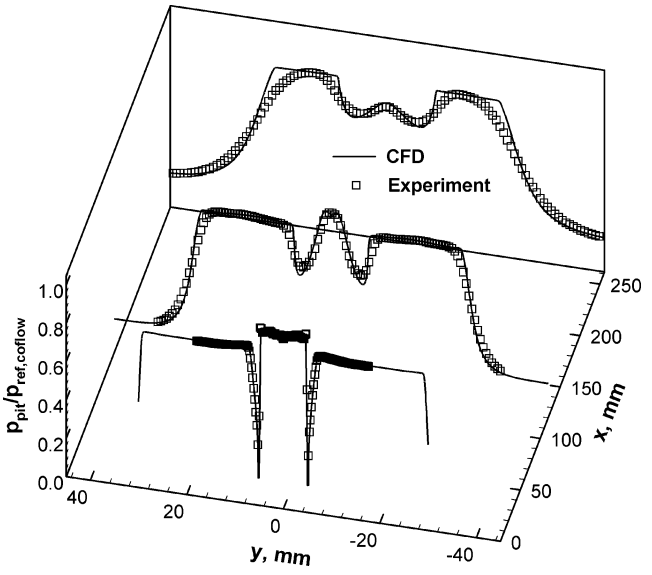

Fig. 7 Comparison of pitot pressure measurements with CFD.

extension ring is in place so the entrained ambient air impinges at only about 39 deg and the shock is much weaker. Despite all of these features, the CFD calculation shows that the center-jet core Mach number remains within ± 0.1 of 1.8, except within the abovementioned shock-expansion waves, out to about $x = 200$ mm.

Figure 8 shows the measured surveys of mole fraction of center-jet gas. The data are smooth and symmetrical and show the radial growth of the mixing layer and plume. The y locations where $\chi_{\mathrm{He-O2}} = 0.01$ and $\chi_{\mathrm{He-O2}} = 0.99$, on both sides of the axis, are interpolated from the data, and the magnitudes are taken: $\delta_{0.01}, \delta_{0.99}$. The results are plotted as a function of x in Fig. 9, along with straight line fits. The thickness of the two-stream mixing layer between the center jet and coflow, upstream of $x = 148$ mm, where $\delta_{0.99} > 0$, is defined as $\delta_{0.01} - \delta_{0.99}$. The rate of change of this thickness or "growth rate" is 0.0654. The visual thickness, widely used in the literature, is the thickness between two straight lines marking the limits of the mixing layer on each side, found by flow visualization methods such as schlieren. Papamoschou and Roshko[8] provide an equation for the growth rate of the "visual thickness" of an incompressible mixing layer as a function of velocity ratio and density ratio between the two streams. The incompressible growth rate computed is 0.151 for our experiment, and the ratio of the experimental growth rate to the computed rate is 0.43. This ratio is in the middle of the spread of

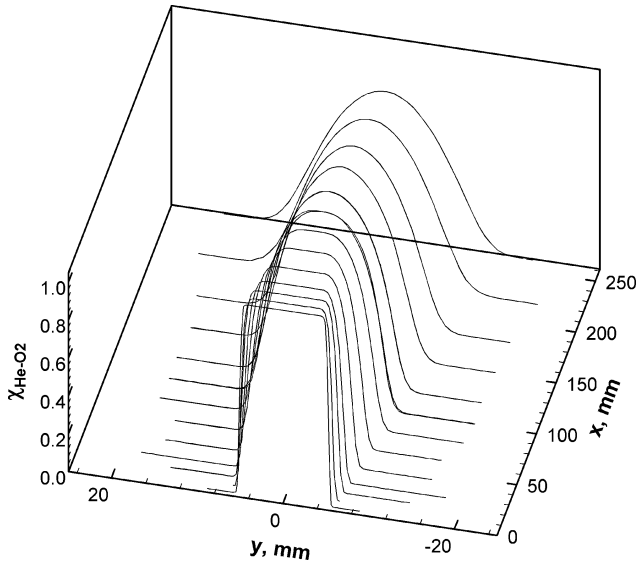

Fig. 8 Mole fraction center-jet gas measurements.

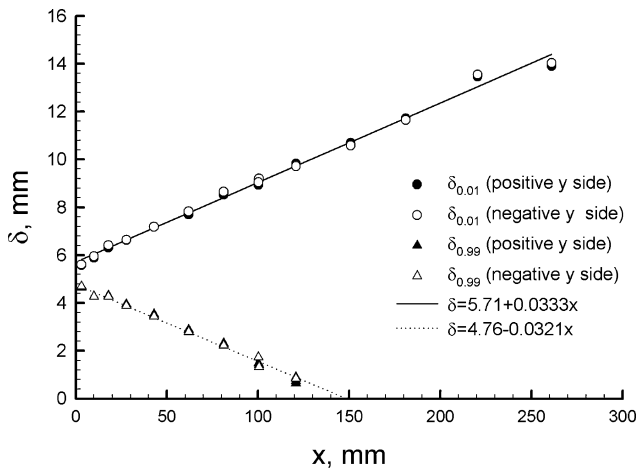

Fig. 9 Boundaries of the mixing region(1 and 99% mol fraction).

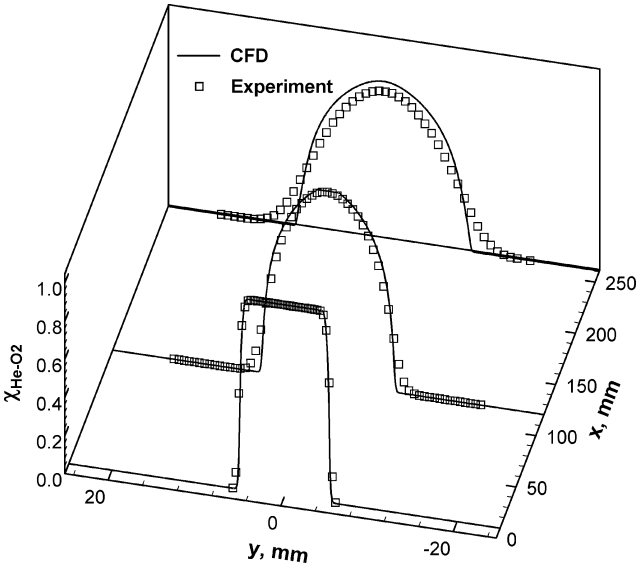

Fig. 10 Comparison of mole fraction measurements with CFD.

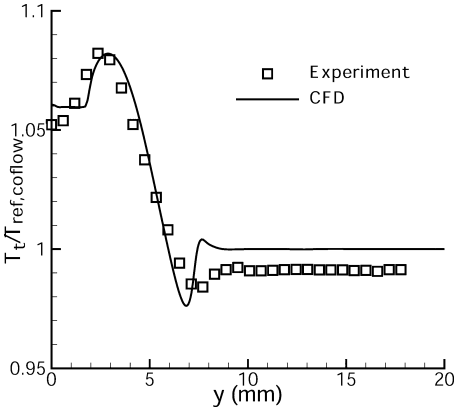

Fig. 11 Comparison of total temperature measurements with CFD at $x = 100.6$ mm.

reported values in the literature at the experimental M_c of 0.70, as reported by, for example, Rossman et al.[10] and Dimotakis.[7]

At $x = 151$ mm the peak mole-fraction center-jet gas, which occurs on the centerline, begins to fall below 1, reaching about 0.77 at $x = 261$ mm. This is the plume region of the flow. Within this region, the outer boundary of the plume, $\delta_{0.01}$, continues to grow at the same linear rate.

Figure 10 shows comparisons between the calculations and the experiment. Moving away from the axis, the calculation is first high and then, approaching $\chi_{He-O2} = 0$, too low. The calculation is also nearly discontinuous in slope at $\chi_{He-O2} = 0$ (a most unphysical behavior).

Figure 6 shows the measured surveys of pitot pressure. The pitot pressure is slightly higher in the center jet than in the coflow and is low in the stagnant air surrounding the jet. At $x = 0.13$ mm there is a layer of low pitot pressure, several times the thickness of the centerbody lip, that results from the merging of the boundary layers from the centerbody surfaces and the region of separation at the lip. Downstream, the region of mixing between the center jet and coflow may be observed as a region of low pitot pressure. Small axisymmetric irregularities in pitot pressure in the center jet and the coflow "freestreams," seen particularly in the first four planes, are attributed to the previously described wave systems emanating from the centerbody lip. Figure 7 shows comparisons between the calculations and the experiment. The agreement at $x = 0.13$ mm is very good, indicating that the calculation of the flow in the nozzles was good. Downstream of $x = 0.13$ mm the agreement is poorer: moving out from the axis the calculation is low near the pitot pressure minimum, then high either side of the coflow freestream.

Total temperature data were acquired only at $x = 101$ mm. Comparisons of this data with CFD are shown in Fig. 11. Both on the axis and in the coflow freestream, experimental data are about 1% below the known supply-gas temperatures. This discrepancy is probably due to probe error (i.e., the "recovery factor" of the probe is not quite 100%, which is normal for this type of probe). Otherwise, the quality of agreement between calculations and experiment is fair, with the calculations reproducing the observed overshoot and undershoot of total temperature relative to freestream values.

Figure 12 shows the mean RELIEF velocity data. The velocity is significantly higher in the center jet than in the coflow. At $x = 2$ mm, the layer that results from the merging of the boundary layers from the centerbody surfaces and the region of separation at the lip may be seen as a region of varying velocity that undershoots the coflow freestream. The mean velocity distribution in the center jet near the nozzle exit is not perfectly uniform because of the previously described wave system emanating from the nozzle lip. Downstream of the nozzle exit, the center jet spreads in a manner qualitatively similar to χ_{He-O2}, but the drop in velocity near the axis below the nozzle-exit value (end of the potential core) begins significantly farther upstream of the point where χ_{He-O2} drops below 1, near $x = 62$ mm (instead of $x = 151$ mm). Comparisons of the mean velocity with CFD calculations are shown in Fig. 13. In this figure, the velocity is normalized by the calculated center-jet nozzle exit velocity $U_{nom} = 1127$ m/s. Agreement is good at $x = 2$ mm, but downstream of this point the calculations are consistently high near the center of the center jet and low at the edge.

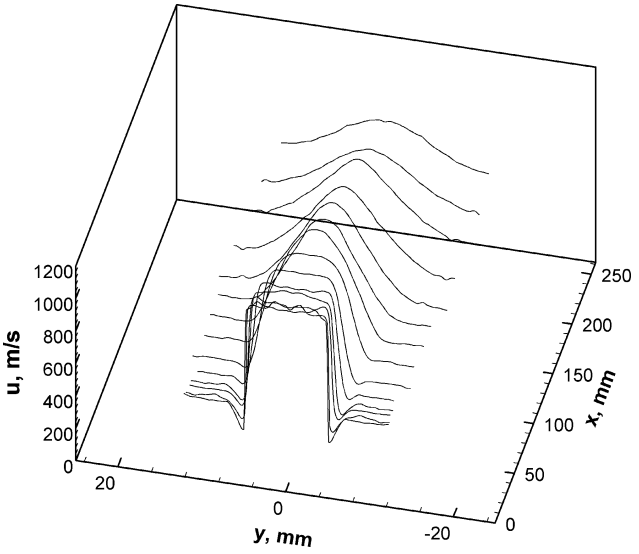

Fig. 12 RELIEF mean velocity measurements.

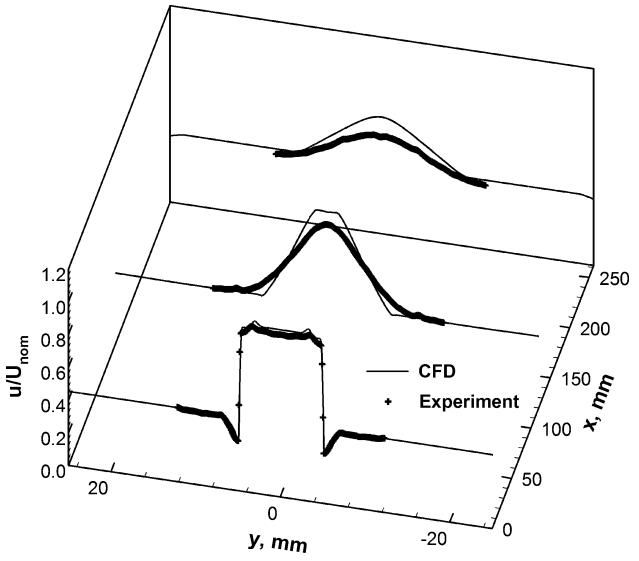

Fig. 13 Comparison of RELIEF mean velocity measurements with CFD.

The experimental rms x-component velocity fluctuation data are shown in Fig. 14. Data rise above a baseline of about 10–15 m/s, which is the precision error in the RELIEF measurements of instantaneous velocity. Because the precision errors and true velocity fluctuations are uncorrelated, $\overline{u'^2}$ is measured consistently high by roughly $(15\ \text{m/s})^2$, and the rms is high by less than 15 m/s, roughly according to the equation

$$\text{error}\left(\sqrt{\overline{u'^2}}\right) = \sqrt{\overline{u'^2} + 15^2} - \sqrt{\overline{u'^2}}$$

The peak rms fluctuation level at $x = 2$ mm is 120 m/s, but peak levels drop rapidly downstream. This measurement, where the shear layer is only a few pixels thick, is unreliable because of lack of spatial resolution. Comparisons between the measured $\sqrt{\overline{u'^2}}$ and $\sqrt{[(2/3)\tilde{k}]}$ derived from the CFD calculations, where $\tilde{k}$ is the turbulent kinetic energy, are shown in Fig. 15. (Velocity fluctuations are also normalized by the calculated center-jet nozzle exit velocity.) In isotropic turbulence these two quantities are equal; in most turbulent shear flows $\sqrt{\overline{u'^2}}$ is a little greater than $\sqrt{[(2/3)\tilde{k}]}$ (Refs. 13, 14, and 28). The calculated peak amplitudes are roughly consistent with the data; however, the width of the mixing layer is seriously underpredicted by the calculation. Furthermore, the data show that fluctuation levels in the coflow freestream rise moving downstream but levels in the calculation are zero.

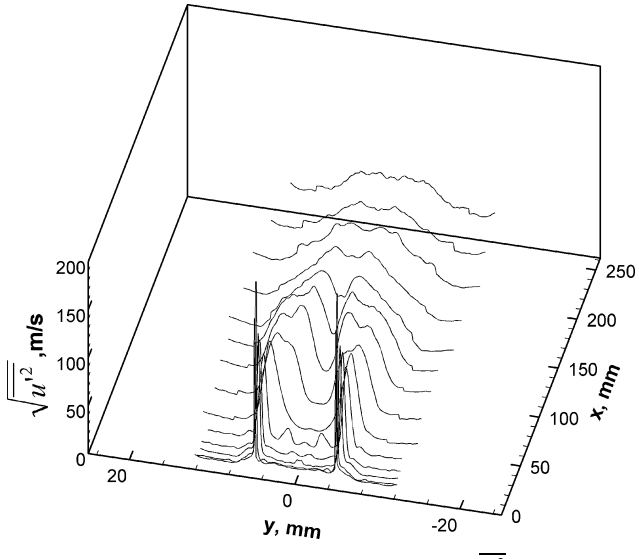

Fig. 14 RELIEF measurements of $\sqrt{\overline{u'^2}}$.

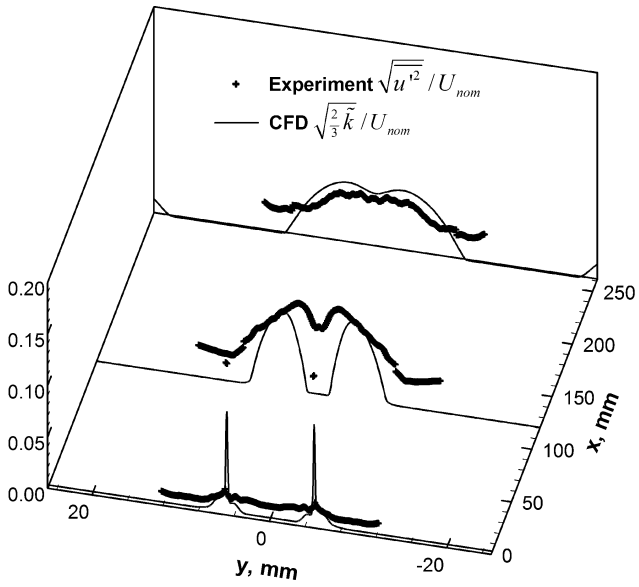

Fig. 15 Comparison of RELIEF measurements of $\sqrt{\overline{u'^2}}$ with CFD calculations of $\sqrt{[(2/3)\tilde{k}]}$.

Additional calculations utilizing the methods described herein are reported in Refs. 3 and 6. In Ref. 3 Pr_T and Sc_T were varied, the effects of compressibility and Pope's corrections were considered, and other turbulence models were tried. In Ref. 6 a parameter that regulates the diffusion of turbulent kinetic energy (σ^* in Wilcox's nomenclature) was also varied. It was found that optimal values of Sc_T and Pr_T are in the range 0.75–0.8, although this flow is more sensitive to Sc_T than to Pr_T . This is consistent with the previously cited results of Calhoon et al.[16] in which Sc_T and Pr_T were roughly 0.2 at $M_c = 0.27$ and 0.9 at $M_c = 1.3$. (Recall that $M_c = 0.70$ in our experiment.) It was also found that the calculations of all quantities, particularly at the boundaries of the coflow freestream, could be greatly improved by increasing σ^* from Wilcox's recommended value of 0.5 to roughly 1.0, increasing the spreading of the turbulent kinetic energy. This change to σ^* is merely an ad hoc correction that would likely produce poorer results in some of the incompressible and boundary-layer flows for which the model coefficients were originally set. For this reason, those results are not presented herein.

As a final comment, it should be noted that the data described herein are available in electronic format to individuals seeking to use it for development or validation of their codes or models. Contact the first author.

Summary

This paper describes an experiment to obtain data for the development and calibration of turbulence models for CFD codes. This experiment was a study of a coaxial jet discharging to the laboratory in which the center jet is a He–O_2 mixture and the coflow jet is air. Both nozzle-exit flows were Mach 1.8 and nearly one dimensional, whereas the mixing layer between them was compressible with a convective Mach number of 0.70. The coaxial-jet flow was uniform and nearly shock free. Flowfield measurements were acquired at the nozzle-exit plane and in the jet downstream, with sufficient detail and accuracy for code validation. Techniques included schlieren flow visualization, gas sampling and analysis, pitot and total-temperature probe surveys, and RELIEF flow-tagging velocimetry. Model geometry and boundary conditions were well characterized. The center-jet/coflow mixing-layer growth rate was reduced to 43% of the incompressible value, consistent with the results of many studies of planar mixing layers at this convective Mach number.

A CFD calculation is also described that utilized a structured finite-difference code (Vulcan) and Wilcox's $\tilde{k}$–$\tilde{\omega}$ model. A constant turbulent Schmidt number of 0.75 was found to be effective. The calculations of various quantities deviated from the experiment near the boundary of the coflow freestream with the mixing layer. This problem could be corrected by increasing the radial diffusion of turbulent kinetic energy.

Acknowledgment

The authors acknowledge the support of the Hypersonic Airbreathing Propulsion Branch of the NASA Langley Research Center.

References

[1]Carty, A. A., and Cutler, A. D., "Development and Validation of a Supersonic Helium–Air Coannular Jet Facility," NASA CR-1999-209717, Nov. 1999.

[2]Cutler, A. D., Carty, A. A., Doerner, S. E., Diskin, G. S., and Drummond, J. P., "Supersonic Coaxial Jet Flow Experiment for CFD Code Validation," AIAA Paper 99-3588, July 1999.

[3]Cutler, A. D., and White, J. A., "An Experimental and CFD Study of a Supersonic Coaxial Jet," AIAA Paper 2001-0143, Jan. 2001.

[4]Drummond, J. P., Diskin, G. S., Cutler, A. D., and Danehy, P. M., "Fuel–Air Mixing and Combustion in Scramjets," AIAA Paper 2002-3878, July 2002.

[5]Cutler, A. D., Diskin, G. S., Danehy, P. M., and Drummond, J. P., "Fundamental Mixing and Combustion Experiments for Propelled Hypersonic Flight," AIAA Paper 2002-3879, July 2002.

[6]Cutler, A. D., Danehy, P. M., O'Byrne, S., Rodriguez, C. G., and Drummond, J. P., "Supersonic Combustion Experiments for CFD Model Development and Validation," AIAA Paper 2004-0266, Jan. 2004.

[7]Dimotakis, P. E., "Turbulent Free Shear Layer Mixing and Combustion," *High-Speed Flight Propulsion Systems*, edited by S. N. B. Murthy and E. T. Currran, Vol. 137, Progress in Astronautics and Aeronautics, AIAA, Washington, DC, 1991, pp. 265–340.

[8]Papamoschou, D., and Roshko, A., "The Compressible Turbulent Shear Layer: An Experimental Study," *Journal of Fluid Mechanics*, Vol. 197, 1988, pp. 453–477.

[9]Rossmann, T., Mungal, M. G., and Hanson, R. K., "Evolution and Growth of Large-Scale Structures in High Compressibility Mixing Layers," *Journal of Turbulence* [online journal], Vol. 3, No. 9, 2002, pp. 1–19; URL: http://jot.iop.org/.

[10]Rossmann, T., Mungal, M. G., and Hanson, R. K., "Character of Mach Wave Radiation and Convection Velocity Estimation in Supersonic Shear Layers," AIAA Paper 2002-2571, June 2002.

[11]Thurow, B. S., Blohm, M., Lempert, W. R., and Samimy, M., "High Repetition Rate Planar Velocity Measurements in a Mach 2.0 Compressible Axisymmetric Jet," AIAA Paper 2005-515, Jan. 2005.

[12]Clemens, N. T., and Mungal, M. G., "Large-Scale Structure and Entrainment in the Supersonic Mixing Layer," *Journal of Fluid Mechanics*, Vol. 284, 1995, pp. 171–216.

[13]Samimy, M., and Elliott, G. S., "Effects of Compressibility on the Characteristics of Free Shear Layers," *AIAA Journal*, Vol. 28, No. 3, 1990, pp. 439–445.

[14]Goebel, S. G., and Dutton, J. C., "Experimental Study of Compressible Turbulent Mixing Layers," *AIAA Journal*, Vol. 29, No. 4, 1991, pp. 538–546.

[15]Baurle, R. A., "Modeling of High Speed Reacting Flows: Established Practices and Future Challenges," AIAA Paper 2004-267, Jan. 2004.

[16]Calhoon, W. H., Arunajatesan, S., and Dash, S. M., "Heat Release and Compressibility Effects on Planar Shear Layer Development," AIAA Paper 2003-1273, Jan. 2003.

[17]Miles, R. B., Grinstead, J., Kohl, R. H., and Diskin, G. S., "The RELIEF Flow Tagging Technique and Its Application in Engine Testing Facilities and for Helium–Air Mixing Studies," *Measurement Science Technologies*, Vol. 11, 2000, pp. 1272–1281.

[18]Gutmark, E., Schadow, K. C., and Wilson, K. J., "Effect of Convective Mach Number on Mixing of Coaxial Circular and Rectangular Jets," *Physics of Fluids A.*, Vol. 3, No. 1, 1991, pp. 29–36.

[19]Murukami, E., and Papamoschou, D., "Eddy Convection in Coaxial Supersonic Jets," *AIAA Journal*, Vol. 38, No. 4, 2000, pp. 628–635.

[20]Zucrow, M. J., and Hoffman, J. D., *Gas Dynamics, Vol II: Multidimensional Flow*, Krieger, Malabar, FL, 1985, pp. 87–103.

[21]Harris, J. E., and Blanchard, D. K., "Computer Program for Solving Laminar, Transitional, or Turbulent Compressible Boundary-Layer Equations for Two-Dimensional and Axisymmetric Flow," NASA TM 83207, Feb. 1982.

[22]Wilcox, D. C., *Turbulence Modeling for CFD*, 2nd ed., DCW Industries, La Canada, CA, 1998.

[23]Cutler, A. D., and Johnson, C. H., "Analysis of Intermittency and Probe Data in a Supersonic Flow with Injection," *Experiments in Fluids*, Vol. 23, No. 1, 1997, pp. 38–47.

[24]Eckbreth, A. C., *Laser Diagnostics for Combustion Temperature and Species*, 2nd ed., Gordon and Breach, Amsterdam, 1996, pp. 20, 21.

[25]Drummond, J. P., "A Two-Dimensional Numerical Simulation of a Supersonic, Chemically Reacting Mixing Layer," NASA TM 4055, Dec. 1988.

[26]Carpenter, M. H., "Three-Dimensional Computations of Cross-Flow Injection and Combustion in a Supersonic Flow," AIAA Paper 89-1870, June 1989.

[27]White, J. A., and Morrison, J. H., "A Pseudo-Temporal Multi-Grid Relaxation Scheme for Solving the Parabolized Navier–Stokes Equations," AIAA Paper 99-3360, June 1999.

[28]Hinze, J. O., *Turbulence*, 2nd ed., McGraw–Hill, New York, 1975, Chap. 6.

K. Ghia
Associate Editor